A Tryptophan-Rich Hexapeptide Inhibits Nucleic Acid Destabilization Chaperoned by the HIV-1 Nucleocapsid Protein†

Chinappan Raja,‡ Jan Ferner,§ Ursula Dietrich,|| Sergiy Avilov,‡,⊥ Damien Ficheux,# Jean-Luc Darlix,△ Hugues de Rocquigny,‡ Harald Schwalbe,§ and Yves Mély*,‡

Département Pharmacologie et Physicochimie, Faculté de Pharmacie, Institut Gilbert-Laustriat, UMR 7175 CNRS/Université Louis Pasteur (Strasbourg I), 74 route du Rhin, 67401 Illkirch, France, Institute for Organic Chemistry and Chemical Biology, Center for Biomolecular Magnetic Resonance, Johann Wolfgang Goethe University, Marie Curie Strasse 11, 60439 Frankfurt am Main, Germany, Georg Speyer Haus, Institute for Biomedical Research, Paul Ehrlich Strasse 42-44, 60596 Frankfurt, Germany, Palladin Institute of Biochemistry, 9, Leontovich Street, 01030 Kiev, Ukraine, IBCP, 7, passage du Vercors, 69367 Lyon Cedex 07, France, and LaboRétro, Unité de Virologie Humaine INSERM 412, Ecole Normale Supérieure de Lyon, 46 allée d'Italie, 69364 Lyon, France

Received December 16, 2005; Revised Manuscript Received April 13, 2006

ABSTRACT: The nucleocapsid protein (NC) of HIV-1 exerts critical functions in viral genome replication and virus assembly. Since the recognition of target nucleic acids is required in the initial step of most NC-mediated processes, attempts were made to find small molecules capable of competing with this recognition. In particular, several Trp-rich hexapeptides were recently found to strongly bind RNA sequences targeted by NC. To further validate these peptides as potential anti-NC agents, we studied the ability of Ac-HKWPWW-NH_2, taken as a representative, to interfere with the NC chaperone properties required during reverse transcription. Using NMR and steady-state and time-resolved fluorescence spectroscopy, we characterized the structure of Ac-HKWPWW-NH_2 as well as its binding to viral sequences such as TAR and PBS involved in the two obligatory strand transfers of reverse transcription. Results show that Ac-HKWPWW-NH_2 exhibits an almost symmetric *cis*−*trans* equilibrium at the level of the Pro residue where it is structured. The peptide binds both TAR and PBS sequences with low micromolar affinities. The *cis*-Pro and *trans*-Pro conformations of the peptide bind with comparable affinities to (−)PBS, mainly through stacking interactions between the Trp residues and the (−)PBS bases. Though all three Trp residues may contribute to the (−)PBS/Ac-HKWPWW-NH_2 complex formation, Trp3 and Trp5 residues are the key residues in the complexes with the *cis*-Pro and *trans*-Pro conformations, respectively. Moreover, Ac-HKWPWW-NH_2 stabilizes cTAR secondary structure and largely inhibits the NC-directed melting of cTAR. This further strengthens the interest of this peptide for deriving modified peptides capable of inhibiting NC and HIV-1 replication.

The nucleocapsid protein (NC)[1] of the human immunodeficiency virus type 1 (HIV-1) plays several key roles in the viral life cycle, either as a domain of the Gag polyprotein precursor or as the mature protein. NC notably selects and directs dimerization of the genomic RNA, which is subsequently efficiently packaged into assembling viral particles (*1*, *2*). Moreover, NC acts as a chaperone protein during reverse transcription by promoting the annealing of the primer tRNA to the primer binding site (PBS) and directing the two obligatory strand transfers necessary for the synthesis of a complete proviral DNA by reverse transcriptase (*3*−*10*). In the first transfer, the cTAR from the strong stop cDNA [(−)sscDNA] is hybridized to the TAR located at the 3′ end of the genomic RNA while the second transfer occurs via the annealing of the (+)PBS and (−)PBS sequences located at the 3′ end of the (+)ssDNA and cDNA(−), respectively.

The mature nucleocapsid protein is a small highly basic protein with two $CX_2CX_4HX_4C$ zinc fingers connected by a short flexible basic linker (*11*). Zinc fingers are essential for

† The Agence Nationale de Recherches sur le SIDA (ANRS), the European TRIOH Consortium, the Deutsche Forschungsgemeinschaft (SFB579 on RNA-Ligand Interactions), the Center for Biomolecular Magnetic Resonance, and the State of Hesse are gratefully acknowledged for financial support to this work. C.R. was a fellow from Sidaction. S.A. was a fellow from the French Ministère de la Recherche and Fondation pour la Recherche Médicale.

* To whom correspondence should be addressed. Tel: +33 (0)3 90 24 42 63. Fax: +33 (0)3 90 24 43 12. E-mail: yves.mely@pharma.u-strasbg.fr.

‡ Institut Gilbert-Laustriat.

§ Johann Wolfgang Goethe University.

|| Institute for Biomedical Research.

⊥ Palladin Institute of Biochemistry.

IBCP.

△ Ecole Normale Supérieure de Lyon.

[1] Abbreviations: DQF-COSY, double-quantum-filtered correlation spectroscopy; Fl, fluorescein; HIV-1, human immunodeficiency virus type 1; HSQC, heteronuclear single-quantum correlation; MES, 2-(*N*-morpholino)ethanesulfonic acid; NC, nucleocapsid protein; NMR, nuclear magnetic resonance; PAGE, polyacrylamide gel electrophoresis; PBS, primer binding site; ROE, rotating-frame Overhauser enhancement; ROESY, rotating-frame Overhauser enhancement spectroscopy; SL3, stem−loop 3 from the Psi encapsidation sequence of the HIV-1 genome; TAR, transactivation response element; cTAR, complementary DNA sequence to TAR; TMR, 5- and 6-carboxytetramethylrhodamine; TOCSY, total correlated spectroscopy.

10.1021/bi052560m CCC: $33.50
Published on Web 07/07/2006

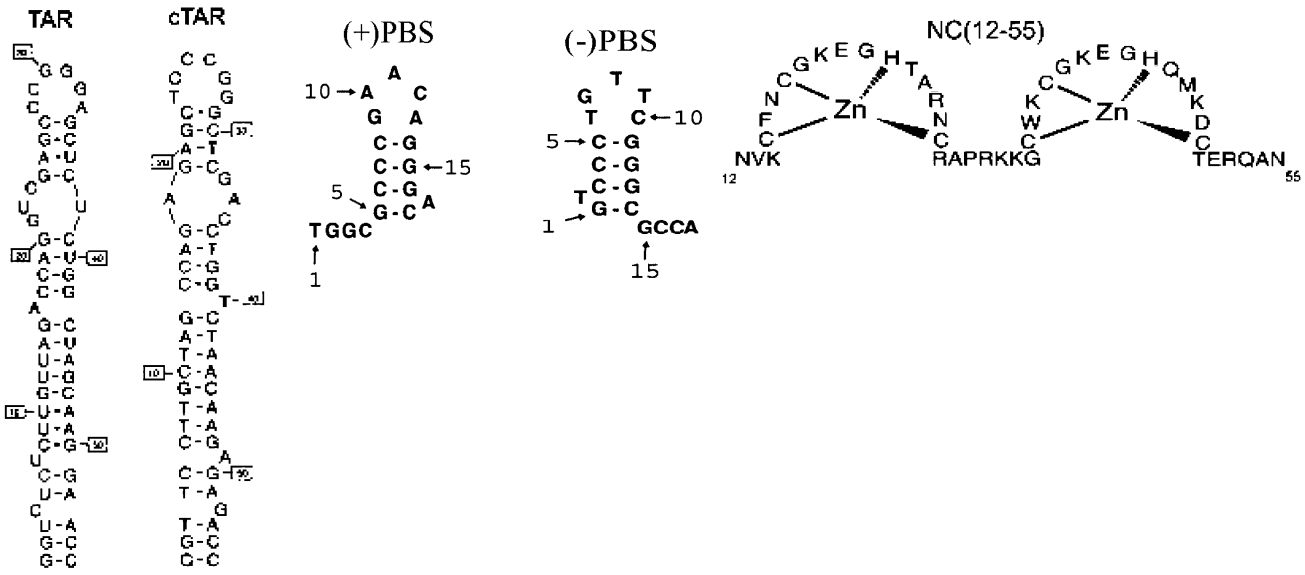

FIGURE 1: Structure of TAR RNA, cTAR DNA, (+)PBS DNA, (−)PBS DNA, and NC(12−55). The selected TAR and PBS sequences are from the HIV-1 Mal strain. The secondary structures of cTAR and PBS were predicted from that of TAR (*72*) and (−)PBS (*73*), respectively, and the mfold program (*74*).

NC activities. Indeed, mutations of amino acids involved in zinc binding completely abolish virus infectivity and impair virion structure (*12*−*15*). The NC mutant virions have low amounts of genomic RNA and exhibit defects in reverse transcription (*10*, *12*, *13*, *16*−*22*). These results were corroborated by in vitro studies describing the NC determinants in nucleic acid binding and chaperone activities (*13*, *19*, *20*, *23*−*25*). Nucleic acid chaperoning by NC is thought to involve at least three steps: (i) binding of NC to its target nucleic acid sequences, (ii) destabilization of the nucleic acid secondary and tertiary structures, and (iii) promotion of the annealing of the destabilized complementary sequences (for a review, see ref *5* and references cited therein). NC destabilization properties mainly rely on the zinc fingers while NC-mediated annealing depends also on the basic amino acids located in both N- and C-terminal regions (*13*, *19*, *20*, *23*−*25*).

Due to its numerous functions in the viral life cycle and its highly conserved sequence, NC constitutes an attractive target for the development of antiviral agents (*26*−*30*). In this respect, many attempts were performed to target directly NC molecules with either (i) zinc-ejecting agents that react with Cys residues within the zinc fingers and induce subsequent loss of functionally active conformation (*31*) or (ii) RNA aptamers and xanthenyl ring-containing compounds that bind NC with high affinity (*32*−*35*). Since the initial step of most NC-promoted activities corresponds to a nucleic acid recognition process, an alternative strategy is to synthesize small molecules able to compete with NC to its target nucleic acids. In this respect, phage display libraries were recently used to identify small peptides able to interact with the encapsidation ψ RNA sequence of HIV-1 (*36*). This study identified Trp-rich hexapeptides that bind with micromolar affinities to the encapsidation sequence of the genomic RNA and may thus potentially interfere with the selection, dimerization, and packaging of the HIV-1 genome.

To further validate the potential of these Trp-rich peptides to interfere with NC functions during reverse transcription, we performed a detailed structural and functional analysis of Ac-HKWPWW-NH_2, taken as a representative of these peptides. The structure of this peptide and its interaction with (−)PBS DNA were studied by NMR. Moreover, steady-state and lifetime fluorescence spectroscopy was used to further characterize its binding to the TAR (TAR RNA and cTAR DNA) and PBS [(−)PBS DNA and (+)PBS DNA] sequences (Figure 1) involved in the first and second strand transfers during reverse transcription. In addition, using doubly labeled cTAR DNA sequences, we characterized the ability of Ac-HKWPWW-NH_2 to inhibit the NC-directed destabilization of the cTAR secondary structure. Taken together, our results show that this peptide exhibits an almost symmetric *cis*−*trans* equilibrium at the level of its Pro residue, binds to both TAR and PBS sequences with low micromolar affinities mainly through stacking interactions with Trp residues, stabilizes the secondary structure of cTAR, and inhibits its NC-mediated melting in vitro. This further strengthens the importance of this peptide to derive modified peptides or small molecules able to inhibit NC functions during HIV-1 replication.

MATERIALS AND METHODS

NC(12−55) (Figure 1) and Ac-HKWPWW-NH_2 were synthesized by solid-phase chemistry as previously described (*36*, *37*). The peptides were purified on reversed-phase HPLC columns and lyophilized. NC(12−55) was stored in its zinc-bound form, and its concentration was determined using an extinction coefficient of 5700 M^{-1} cm^{-1} at 280 nm.

Doubly and singly labeled DNA oligonucleotides were synthesized at a 0.2 μmol scale by IBA GmbH Nucleic Acids Product Supply (Göttingen, Germany). For this study, we used a pair of dyes, 5- and 6-carboxytetramethylrhodamine (TMR) and 5- and 6-carboxyfluorescein (Fl) (*38*). The 5′ terminus was labeled with TMR via an amino linker with a six carbon spacer arm. The 3′ terminus was labeled with Fl using a special solid support with the dye already attached. Oligonucleotides were purified by PAGE, and the purity was verified by electrospray ionization mass spectrometry. Fluorescence experiments were performed in 25 mM Tris-HCl,

pH 7.5, 30 mM NaCl, and 0.2 mM $MgCl_2$ (*25*, *38*, *39*). Concentrations of oligonucleotides and peptides were measured by UV absorption on a Cary 400 UV−visible spectrophotometer. Extinction coefficients of 521910, 396600, 153900, and 175680 M^{-1} cm^{-1} at 260 nm were used for cTAR, TAR, (−)PBS, and (+)PBS sequences, respectively (*10*, *38*). All experiments were performed at 20 °C. Ac-HKWPWW-NH_2−cTAR binding, the effect of Ac-HKWPWW-NH_2 on NC destabilizing activity, and NMR spectra of Ac-HKWPWW-NH_2 were also studied at 37 °C.

Homo- and Heteronuclear NMR Measurements. For the structure determination of the peptide, NMR experiments were recorded at 298 and 310 K on a 2.0 mM Ac-HKWPWW-NH_2 peptide sample which was synthesized as described above with an N-terminal acetylation and an amide group at the C-terminus. The NMR buffer contained 25 mM potassium phosphate and 50 mM potassium chloride, and the pH was adjusted to 6.2. NMR resonance assignment was accomplished by analyzing the following experiments: a ^1H,^{15}N HSQC and a ^1H,^{13}C HSQC (*40*−*42*) a ^1H,^1H DQF-COSY, a ^1H,^1H TOCSY (*43*) (mixing time of 80 ms), and a ^1H,^1H ROESY (*44*) (mixing time of 400 ms). Full experimental details are provided in the Supporting Information.

The interactions between the peptide and (−)PBS DNA (from MWG-Biotech AG) were monitored by 1D homonuclear ^1H NMR during the titration of a 0.4 mM solution of Ac-HKWPWW-NH_2 with (−)PBS in the above-mentioned NMR buffer. The 1D experiments were recorded with a jump−return−echo sequence where the excitation maximum was set to the chemical shift range of the Trp indole signals. The NMR data were recorded on Bruker 400 and 600 MHz spectrometers at 298 and 310 K.

All structure calculations were performed using the program CNS 1.1 (*45*) and the ARIA 1.2 (*46*) setup and protocols. The protein allhdg 5.3 force field (*47*) was used and was slightly adapted to allow structural calculations with the N-terminal acetyl group, the C-terminal amide, and the *cis*-proline. After each of the first eight iterations, 50 structures were calculated. Then, the ROE distance restraints were recalibrated by ARIA based on the 10 lowest energy structures. The violation tolerance was progressively reduced to 0.1 Å in the last iteration in which 200 structures were calculated. The final 20 lowest energy structures were further analyzed and visualized.

Steady-State and Time-Resolved Fluorescence Measurements. Fluorescence emission spectra were recorded on either a Fluorolog or a FluoroMax spectrofluorometer (Jobin Yvon) equipped with a thermostated cell compartment. The fluorescence quantum yield of Ac-HKWPWW-NH_2 was calculated by using Trp in water as a reference ($\phi_{Trp} = 0.14$) (*48*).

Time-resolved fluorescence spectroscopy measurements were performed with a time-correlated single photon counting technique as previously described (*10*). The excitation wavelengths for Trp and Fl were 295 and 480 nm, respectively, and their emission were monitored at 350 and 520 nm, respectively. The fluorescence lifetime measurements were performed with a 1 μM peptide concentration. Time-resolved data analysis was performed by the maximum entropy method using the Pulse5 software (*49*). The mean lifetime $\langle\tau\rangle$ was calculated from the individual fluorescence lifetimes, τ_i, and their relative amplitudes, α_i, by $\langle\tau\rangle = \sum_i \alpha_i \tau_i$. The population, α_0, of dark species in peptide−oligonucleotide complexes and Fl-5′-cTAR-3′-TMR was calculated by

$$\alpha_0 = 1 - \frac{\langle\tau\rangle_R}{\langle\tau\rangle_S R_m} \quad (1)$$

where $\langle\tau\rangle_R$ is the measured mean lifetime of the free Ac-HKWPWW-NH_2 peptide or the singly labeled Fl-5′-cTAR derivative, while $\langle\tau\rangle_S$ is the measured lifetime of the peptide−oligonucleotide complex or the doubly (Fl-5′-cTAR-3′-TMR) labeled derivative, respectively. R_m corresponds to the ratio of their corresponding steady-state fluorescence intensities. The remaining amplitudes, α_{ic}, were recalculated from the measured amplitudes, α_i, according to $\alpha_{ic} = \alpha_i(1 - \alpha_0)$.

The effect of His1 deprotonation on Ac-HKWPWW-NH_2 fluorescence was monitored in 25 mM 2-(*N*-morpholino)-ethanesulfonic acid (MES) buffer. Direct addition of NaOH to adjust the pH value leads to turbidity, probably due to local peptide precipitation at the point of addition. To avoid this, separated MES buffer solutions with different pH values ranging from 4.5 to 7.5 were prepared. To each solution was added Ac-HKWPWW-NH_2 at a final 1 μM concentration, and its fluorescence intensity at 350 nm was recorded.

For binding studies, fluorescence titrations were performed by adding increasing oligonucleotide concentrations to a fixed amount of peptide in 25 mM Tris-HCl buffer, 30 mM NaCl, and 0.2 mM $MgCl_2$, pH 7.5. The binding stoichiometry was determined at a peptide concentration of 1.5−2.0 μM while the binding constants were determined at peptide concentrations of 0.2−1.5 μM. Fluorescence intensities were corrected for dilution, buffer fluorescence, and screening effects due to the oligonucleotide absorbance. The fluorescence intensity, *I*, at 350 nm was fitted according to

$$I = I_0 - [(I_0 - I_t)/L_t]\{[(1 + (L_t + nN_t)K_{app})] - \sqrt{[(1 + (L_t + nN_t)K_{app})^2] - 4L_t nN_t K_{app}{}^2}\}/2K_{app} \quad (2)$$

where L_t and N_t designate the total concentration of peptide and oligonucleotide, respectively. I_t represents the fluorescence at the plateau when all of the peptide is bound, whereas I_0 and I correspond to the fluorescence intensities of the peptide in the absence and in the presence of a given concentration of oligonucleotide. K_{app} and n correspond to the apparent binding constant and the number of peptide binding sites, respectively.

RESULTS

Characterization of Ac-HKWPWW-NH_2 by NMR. Figure 2 shows the ^1H,^{15}N HSQC spectrum of the peptide. For a single peptide conformation, 10 signals (5 backbone amide resonances, 3 side chain indole resonances, and 2 side chain amide resonances) are expected. The observation of a total of 20 cross-peaks suggests the existence of two conformations in slow chemical exchange; i.e., the rate of interconversion is slow on the NMR time scale (millisecond to second range). The findings of two full and independent data sets described in Figure 2 for the ^1H,^{15}N HSQC are in agreement with the proton 1D spectra and evident in all recorded NMR spectra. By analysis of the ^1H,^1H TOCSY and the ^1H,^1H DQF-COSY spectra, the intraresidual spin systems for both conformers could be assigned. From the

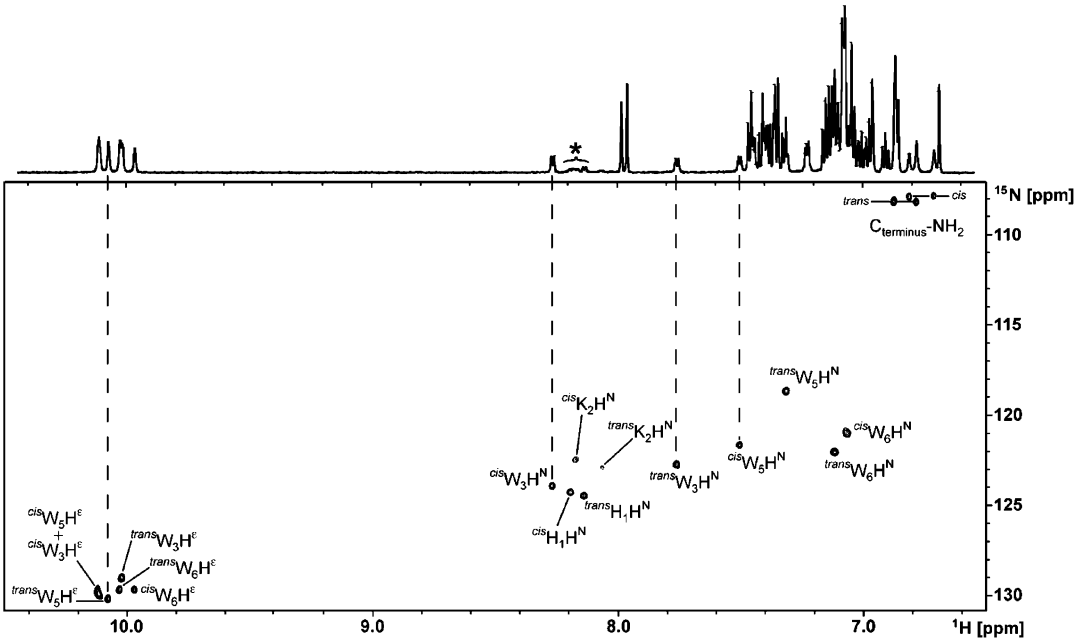

FIGURE 2: NMR spectra of the Ac-HKWPWW-NH_2 peptide. (Top) ^{1}H 1D spectrum of the amide and aromatic region of the peptide recorded at 600 MHz with water presaturation during the relaxation delay. (Bottom) ^{1}H,^{15}N HSQC recorded at 600 MHz showing the assignment of the Trp side chain, the backbone amide, and the C-terminal amide resonances. The labeled signals (*) in the 1D spectrum belong to the backbone amide resonances of the N-terminal residues His1 and Lys2 in both proline conformations. Their weak intensities are due to the water presaturation and indicate a fast exchange with water and no defined structure of the N-terminus.

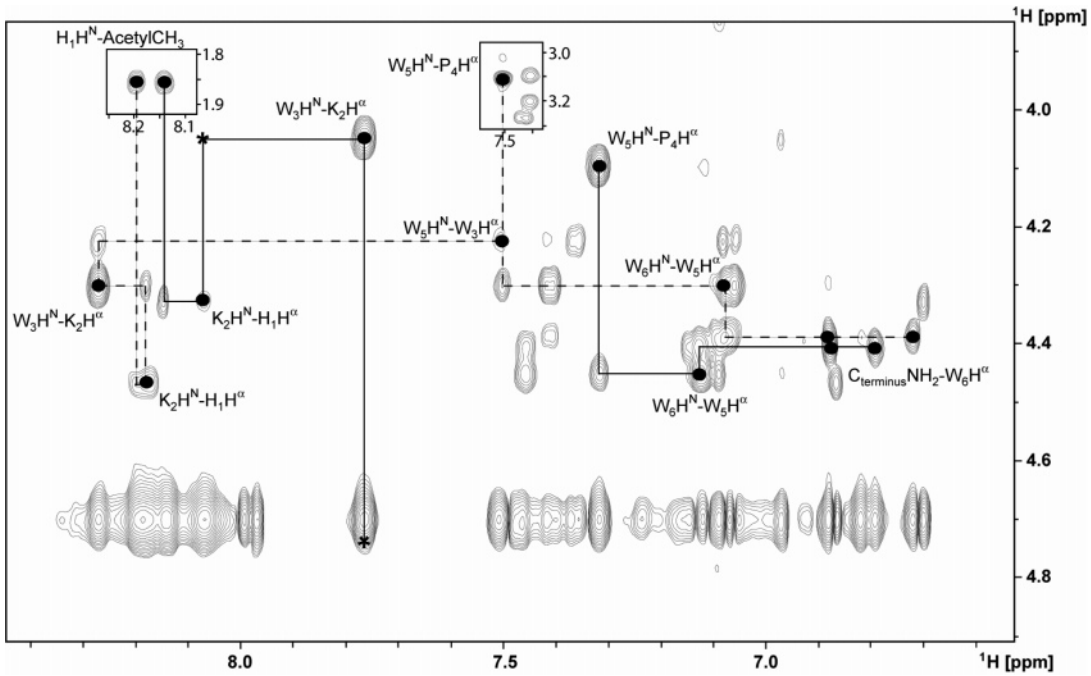

FIGURE 3: $^1H^N$,$^1H^\alpha$ region in the ^{1}H,^{1}H ROESY spectrum of the Ac-HKWPWW-NH_2 peptide. The ROESY spectrum was recorded at 600 MHz with a mixing time of 400 ms. The solid and the dashed lines are the connectivity walks assigned to the *trans*-proline and the *cis*-proline conformations, respectively. The interresidual cross-peaks along the connections are labeled with filled circles (●) and assigned. The intraresidual peaks labeled with an asterisk (*) are observable at lower contour levels and in the TOCSY experiment.

H^N,H^α region of the ^{1}H,^{1}H ROESY spectrum, the spin systems identified in the TOCSY and COSY experiments could be assigned sequentially for each of the two conformations as shown in Figure 3.

The assignment of the two sets of cross-peaks in the 2D NMR spectra to either *cis*- or *trans*-proline conformation was based on the methods of Lee et al. (*50*) and Schubert et al. (*51*). The method of Lee et al. (*50*) derives the Pro conformation from the NOESY patterns around the Pro residue. In the case of the Ac-HKWPWW-NH_2, the ROESY cross-peaks with medium intensity between the H^δs of Pro4 and the H^α proton of the preceding amino acid (Trp3) in one resonance set indicate that the Pro residue likely adopts a *trans* conformation. In contrast, strong cross-peaks from the preceding H^α to the H^α of the proline and medium intensity signals to the amide proton of the following residue (Trp5) indicate a *cis* conformation for the second set of resonances. This assignment is further confirmed by the

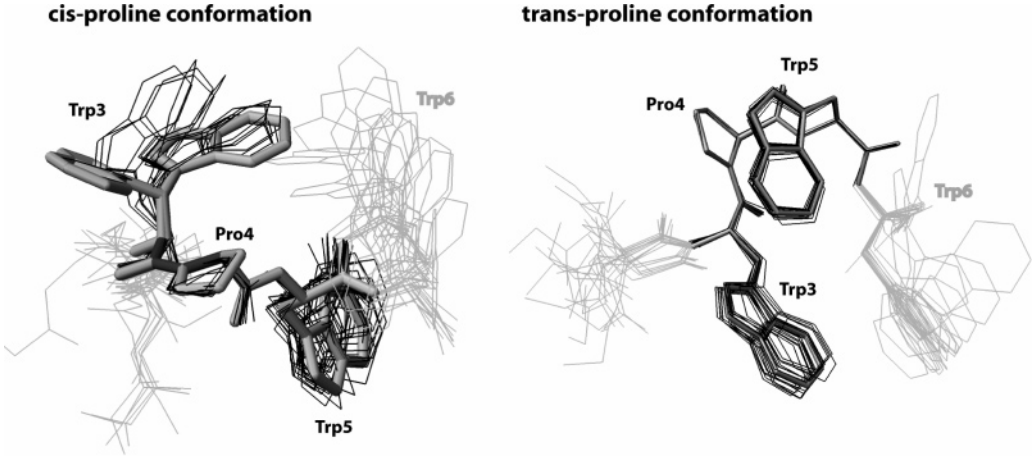

FIGURE 4: Structural ensemble of the two Ac-HKWPWW-NH_2 conformations. The 20 lowest energy structures are shown for both *cis*-proline (left) and *trans*-proline (right) conformations. In both ensembles, the side chains of His1 and Lys2 are not represented since they do not exhibit a preferred conformation. Trp6 shows some preferred conformations and is therefore shaded. The residues in the core region (Trp3−Trp5) are thickened. While in the *trans*-proline conformation, all members of the family of structures superimpose well, the Trp3 side chain in the *cis*-proline conformation wobbles between two conformations.

method of Schubert et al. (*51*), which is based on the chemical shift difference between the carbons at the β-position and at the γ-position of the Pro residue. This chemical shift difference constitutes a reference-independent indicator of the Pro peptide bond conformation based on a statistical analysis of 1033 prolines in 304 proteins deposited in the BioMagRes database. A difference $\Delta_{\beta\gamma} = \delta[^{13}C^{\beta}] - \delta[^{13}C^{\gamma}]$ of around 4.5 ± 1.2 ppm indicates a high probability of a *trans*-proline amide bond conformation, while a difference of 9.6 ± 1.3 ppm is characteristic for the *cis* conformation. The Ac-HKWPWW-NH_2 peptide gives differences of 9.0 and 4.0 ppm for the two observed conformations, in agreement with the ROESY analysis. Peak integration and comparison in 1D and 2D spectra resulted in a *cis*:*trans* ratio of 46:54 with a variation of 4%. Interestingly, no significant change in this ratio was detected when the temperature was raised to 37 °C, indicating that the *cis*−*trans* equilibrium is preserved at physiological temperature.

Analysis of the ROESY spectrum showed no cross-peaks between protons of the two conformations, indicating a slow exchange rate between the two conformations. In addition to the intraresidual ROE cross-peaks, 15 sequential and 4 medium-range (all between Trp3 and Trp5) cross-peaks were observed between the resonances assigned to the *cis* conformation. For the *trans* conformation, 16 sequential resonances and 3 medium-range (from the $H^{\delta}1$ of Trp3 to H^{α} of Trp5 and to one H^{β} of Trp6 as well as from the H^{α} of Pro4 to the backbone H^{N} of Trp6) cross-peaks were observed. The cross-peaks identified in the ROESY spectrum were converted into distance restraints for separate structure calculations using the CNS 1.1 and the ARIA 1.2 programs.

The structure calculations confirmed the results described above. Examination of the 20 lowest energy structures showed a defined structure around the Pro residue in both conformations. The peptide with the *cis*-Pro conformation (Figure 4, left) adopts a folded structure, which is supported by the 4 observed ROE cross-peaks between Trp3 and Trp5. In contrast, the *trans* conformation (Figure 4, right) exhibits an extended backbone. While in the *trans*-Pro conformation both the backbone and the side chains of the residues Trp3, Pro4, and Trp5 can be superimposed, the NMR data for the *cis*-proline conformation suggest that the Trp3 side chain adopts two different conformations. The χ^1 angles of these two conformations are around 60° and slightly above 180°, respectively. The terminal residues, His1, Lys2, and Trp6, exhibit no preferred structure in both conformers.

The average distances and the relative orientations between the aromatic side chains of the Trp residues were determined over the 20 lowest energy structures of both conformations. In the *cis*-Pro conformation, the side chains of Trp5 and Trp6 are about 7−8 Å apart, with a planar orientation. Since the indole ring of Trp3 can adopt two conformations, there is no conserved orientation with respect to the other indole rings and the inter-ring distances are between 7 and 11 Å. Significantly shorter distances between the Trp side chains are observed in the *trans*-Pro conformation. Indeed, in the well-resolved structure of the core of the *trans*-Pro conformation, the indole side chains of Trp3 and Trp5 are only 6.2 (±0.2) Å apart, with a fixed planar orientation. Moreover, Trp6 comes even closer to Trp3 (4.6−6.5 Å) but with no conserved orientation.

Characterization of Ac-HKWPWW-NH_2 by Fluorescence. Trp residues constitute intrinsic fluorescent probes of peptides and proteins. Due to their exquisite sensitivity to the environment, Trp fluorescence properties can be used to obtain information on the overall structural properties and conformational changes of the protein or peptide in which these Trp residues are included (*52*). In this respect, we characterized the fluorescence properties of the three Trp residues in Ac-HKWPWW-NH_2. The fluorescence intensity maximum of Ac-HKWPWW-NH_2 is 351 (±1) nm (Figure 5a), which is typical for fully solvent exposed Trp residues. This, in line with the NMR data, confirms that the three Trp residues do not form a hydrophobic cluster. The fluorescence quantum yield (ϕ) of Ac-HKWPWW-NH_2 in 20 mM Hepes, pH 7.5, buffer was found to be 0.058 (±0.002), which is about 3-fold less than the quantum yield of free Trp (ϕ = 0.14).

Moreover, the time-resolved fluorescence decay of Ac-HKWPWW-NH_2 is characterized by three lifetimes, 0.42, 1.35, and 3.0 ns, with relative amplitudes of 26%, 52%, and 22%, respectively (Table 1). Interestingly, the radiative rate constant, $k_r = \phi/\langle\tau\rangle$, was found to be 3.9×10^7 s^{-1} and thus significantly smaller than that of *N*-acetyl-L-tryptophanamide

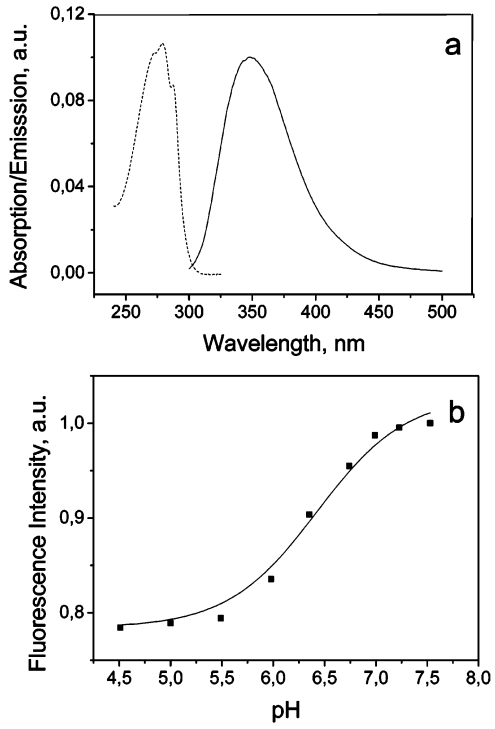

FIGURE 5: Fluorescence characterization of Ac-HKWPWW-NH_2. (a) Absorption and emission spectra of Ac-HKWPWW-NH_2 in 50 mM Hepes, pH 7.5. The dotted and solid lines represent the absorption and emission spectrum, respectively. The excitation wavelength was at 280 nm. (b) Effect of His1 deprotonation on Ac-HKWPWW-NH_2 intrinsic fluorescence. The deprotonation of His1 was monitored through the intrinsic fluorescence of Ac-HKWPWW-NH_2. The experiments were performed in 25 mM MES at different pH values. Excitation and emission wavelengths were 280 and 350 nm, respectively.

in water (*53*), unambiguously indicating static quenching. This quenching may be attributed to ground state stacking interactions that are thought to occur between Trp pairs, notably in the *trans*-proline conformation where the Trp side chains are close.

In a next step, the pK_a of His1 was determined through the pH dependence of the peptide quantum yield. The rationale of this approach is that only the protonated form of His markedly quenches the fluorescence of spatially close Trp residues (*54*, *55*). The quantum yield of Ac-HKWPWW-NH_2 was monitored in 25 mM Mes buffer in the pH range 4.5−7.5 (Figure 5b). We observed a steep decrease in ϕ when the pH decreases. This pH dependence of ϕ was fitted according to (*56*)

$$\phi = \phi_{MH} + (\phi_M - \phi_{MH})/(1 + 10^{pK_a} \times 10^{-pH}) \quad (3)$$

where ϕ_{MH} and ϕ_M are the fluorescence quantum yields of the peptide with protonated and deprotonated His, respectively. A pK_a value of 6.3 (±0.1) close to that of free His was obtained, in line with its random orientation observed by NMR spectroscopy. This indicates that, at pH 7.5, about 95% of the His residues are nonprotonated.

Binding of Ac-HKWPWW-NH_2 to the Viral cTAR and PBS Sequences. To characterize the binding of Ac-HKWPWW-NH_2 to TAR and PBS, reverse titrations were performed by adding increasing oligonucleotide concentrations to a fixed peptide concentration (Figure 6). Binding was monitored through the decrease of Ac-HKWPWW-NH_2 intrinsic fluorescence resulting from the binding to the oligonucleotides. Binding experiments were performed in a 25 mM Tris-HCl, pH 7.5, 30 mM NaCl, 0.2 mM $MgCl_2$ buffer which is currently used for evaluating NC destabilizing properties (*10*, *38*, *39*). For both PBS and TAR derivatives, the titrations indicate a sharp fluorescence decrease that reduces the peptide fluorescence by about 40% and 25% for TAR and PBS derivatives, respectively.

In contrast to the large decrease in the steady-state fluorescence intensity, the three fluorescence lifetimes (0.42, 1.35, and 3.0 ns) and their relative amplitudes remained essentially unchanged upon the formation of the hexapeptide−nucleic acid complexes (Table 1), suggesting the formation of dark species with a very short or null lifetime. These dark species are indicative of stacking interactions between the Trp residues of Ac-HKWPWW-NH_2 and both (+)PBS and cTAR (*57*). Similarly, very low fluorescent species have also been observed with the single Trp residue of NC. However, while these low fluorescent species represent about 90% of the total species in the complexes of NC with its viral nucleic acid targets (*9*, *23*, *58*), the dark species in Ac-HKWPWW-NH_2 complexed with PBS and cTAR represent only 25% and 34%, respectively. This indicates that, in the complexes, only a fraction of the Trp residues of Ac-HKWPWW-NH_2 is stacked with the oligonucleotide bases.

In a first step, the binding stoichiometry of Ac-HKWPWW-NH_2 to the TAR and PBS oligonucleotides was estimated from the intersection of the initial slope of the titration with the fluorescence plateau. The number of binding sites was found to be 7 ± 1 and 12 ± 2 for PBS and TAR derivatives, respectively (Table 2), giving occluded binding sizes of about 2.5 and 4.5 nucleotides per peptide, respectively. These differences in the occluded binding sizes suggest that the Ac-HKWPWW-NH_2 molecules probably do not saturate the TAR species and, thus, that the true occluded binding size for Ac-HKWPWW-NH_2 on oligonucleotides may be equal to or smaller than 2.5. In a second step, the apparent binding constant, K_{app}, was determined by fitting the binding data to eq 2. This approach is only semiquantitative, since it is based on the assumption that the binding sites for the peptide are identical and independent. The binding constant for all TAR derivatives (cTAR DNA, TAR RNA, and its DNA equivalent, TAR DNA) was found to be about 10^6 M^{-1} (Table 2), indicating that there is no strong dependence on the oligonucleotide sequence or nature (DNA or RNA). A similar conclusion also applies for PBS derivatives since Ac-HKWPWW-NH_2 binds to both (+)PBS and (−)PBS sequences with an affinity of (3−4) × 10^6 M^{-1}. Noticeably, the binding constants of Ac-HKWPWW-NH_2 to both TAR and PBS sequences are about 1 order of magnitude higher than those described for related peptides to the SL3 sequence of the encapsidation sequence (*36*). These differences may be ascribed to differences in both the experimental conditions and the peptide sequence since binding of Ac-HKWPWW-NH_2 to SL3 in our conditions led to K_{app} values comparable to those obtained with PBS and TAR (data not shown). Interestingly, though the Ac-HKWPWW-NH_2 peptide contains only six amino acids, its binding constants for both TAR and PBS derivatives are of the same order of magnitude as those reported for NC(12−55) (*9*, *23*). This confirms that this peptide may efficiently compete with NC for its nucleic acid targets.

Table 1: Time-Resolved Fluorescence Parameters of Ac-HKWPWW-NH_2[a]

	α_0	τ_1 (ns)	α_1	τ_2 (ns)	α_2	τ_3 (ns)	α_3	$\langle\tau\rangle$ (ns)
		0.42	0.26	1.35	0.52	3.02	0.22	1.48
(+)PBS	0.25	0.30	0.27 (0.20)	1.28	0.50 (0.38)	2.90	0.23 (0.17)	1.39
cTAR	0.34	0.45	0.30 (0.20)	1.47	0.50 (0.33)	3.08	0.20 (0.13)	1.48

[a] The experiments were performed with 1 μM Ac-HKWPWW-NH_2 either in the absence or in the presence of 1 μM (+)PBS or cTAR. Excitation and emission wavelengths are 295 and 350 nm, respectively. The fluorescence lifetimes, τ_1 to τ_3, the measured relative amplitudes, α_1 to α_3, and the mean lifetime, $\langle\tau\rangle$, are expressed as means for three experiments. The standard errors of the mean are usually below 10% for the lifetimes and 15% for the amplitudes. The relative amplitude, α_0, of the dark species is calculated by eq 1. The remaining amplitudes, α_{ic} (in parentheses), were recalculated according to $\alpha_{ic} = \alpha_i(1 - \alpha_0)$.

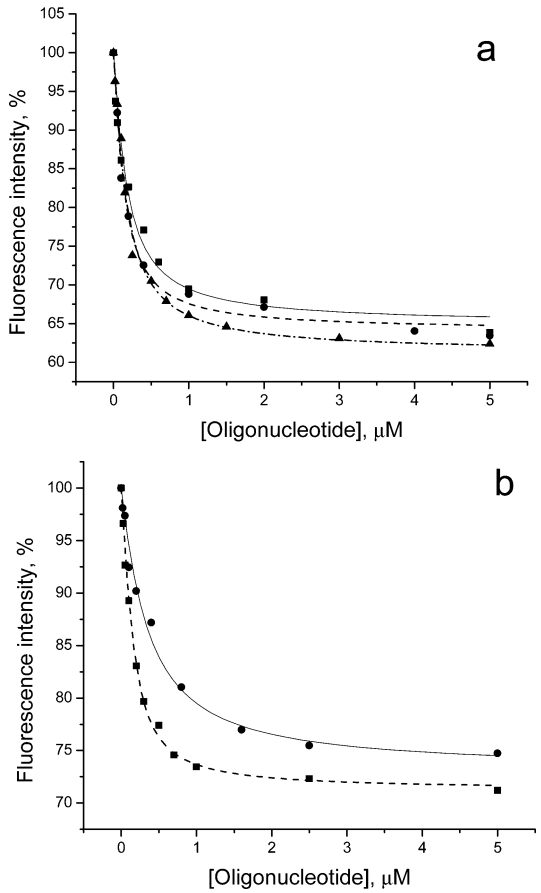

FIGURE 6: Binding curves of Ac-HKWPWW-NH_2 with (a) TAR and (b) PBS derivatives. The peptide concentration was 1 μM in 25 mM Tris-HCl, 30 mM NaCl, and 0.2 mM $MgCl_2$. In (a), the peptide was titrated with TAR RNA (▲, dash−dotted line), TAR DNA (●, dashed line), and cTAR DNA (■, solid line). In (b), the peptide was titrated with (+)PBS (●, solid line) and (−)PBS (■, dashed line). Excitation and emission wavelengths were 295 and 350 nm, respectively. The lines represent the fits of the experimental points with eq 2.

To further characterize the binding process, the salt and temperature dependence of the binding constant of Ac-HKWPWW-NH_2 to cTAR was investigated (*59*). The dependence of the binding constant on NaCl concentration (in the range 30−500 mM) appears very small (data not shown), indicating that the binding strength relies essentially on nonelectrostatic contributions. Moreover, no change in the binding stoichiometry and only moderate affinity decrease (3-fold) of Ac-HKWPWW-NH_2 to cTAR were observed when the temperature was raised to 37 °C, indicating that the hexapeptide can compete with NCp7 for the binding to cTAR also at physiological temperature.

To identify by NMR the peptide conformation which is mostly responsible for the binding to the oligonucleotides,

Table 2: Binding Parameters of Ac-HKWPWW-NH_2 for TAR and PBS Derivatives[a]

sequence	K_{app} ($\times 10^{-6}$) (M^{-1})	n
TAR RNA	1.8	12
cTAR DNA	0.8	12
TAR DNA	1.1	12
(+)PBS	3.0	7
(−)PBS	4.0	7

[a] Experiments were performed in 25 mM Tris-HCl, 30 mM NaCl, and 0.2 mM $MgCl_2$, pH 7.5. The number of binding sites was determined as described in the text. The K_{app} values were calculated by fitting the data in Figure 6 to eq 2. Indicated values correspond to the mean of two to three experiments. The standard error of the mean was usually of 2 for n and about 30% for K_{app}.

Table 3: Chemical Shift Changes of Trp Indole Resonances upon Titration of Ac-HKWPWW-NH_2 with (−)PBS[a]

peptide: DNA ratio	chemical shift changes of Trp indole resonances in the two peptide conformations (ppm)					
	cis W3	cis W5	cis W6	trans W3	trans W5	trans W6
4:1	0.07	0.03	0.05	0.04	0.06	0.05
2:1	0.16	0.08	0.11	0.11	0.14	0.12
1:1	0.24	0.12	0.17	0.16	0.21	0.17
1:4	0.37	0.22	0.28	0.25	0.30	0.26

[a] The experiments were performed with 0.4 mM Ac-HKWPWW-NH_2 and increasing concentrations of (−)PBS at 310 K. The 1D spectra were calibrated on the water signal. The signals overlapping in the 1D experiments were resolved in 2D experiments.

a titration was performed by adding increasing amounts of (−)PBS DNA to a fixed concentration of Ac-HKWPWW-NH_2. Already at the first step of the titration at 298 K where (−)PBS was added to the peptide at a 1:4 molar ratio, a large broadening of all peptide proton signals together with a slight turbidity was observed. This turbidity disappeared when (−)PBS was added to a 1:1 molar ratio, but the signals remained broad and unresolved. The signal intensities and resolution were recovered partly by increasing the temperature to 310 K and by switching to a lower frequency spectrometer (400 MHz). These observations are characteristic of an intermediate exchange of the peptide with the DNA, in line with the binding constant of the peptide to (−)PBS. Moreover, the significant changes of the Trp indole resonances in both *cis*-Pro and *trans*-Pro conformations during titration with (−)PBS (Table 3) indicate that both peptide conformations bind to (−)PBS with comparable affinities. All Trp indole signals shifted upfield during the titration, in line with a stacking of the indole rings with the bases of (−)PBS. In addition, the amplitudes of these shifts can be used to identify which Trp residues are the most important for interaction. In the *cis*-Pro conformation, the large shift displayed by Trp3 suggests that this residue plays a central role in the interaction with (−)PBS. In contrast,

Table 4: Effects of Ac-HKWPWW-NH_2 and NC on cTAR Secondary Structure As Measured by Time-Resolved Fluorescence Spectroscopy[a]

TMR-5′-cTAR-3′-Fl	α_0	τ_1 (ns)	α_1	τ_2 (ns)	α_2	τ_3 (ns)	α_3	$\langle\tau\rangle_S$ (ns)	$\langle\tau\rangle_R$ (ns)	R_m
	0.732	0.16 ± 0.01	0.130	1.23 ± 0.10	0.043	3.92 ± 0.01	0.096	1.77 ± 0.04	3.86	8.1
+NC	0.443	0.15 ± 0.01	0.089	1.30 ± 0.03	0.236	3.7 ± 0.1	0.227	2.27 ± 0.02	3.91	3.1
+Ac-HKWPWW-NH_2	0.852	0.14 ± 0.03	0.052	1.23 ± 0.09	0.020	4.05 ± 0.01	0.075	2.3 ± 0.1	3.95	11.8
+Ac-HKWPWW-NH_2 + NC	0.601	0.30 ± 0.10	0.067	1.42 ± 0.09	0.153	3.7 ± 0.1	0.178	2.3 ± 0.1	3.85	4.2

[a] Experiments were performed in the same buffer as in Table 2. Excitation and emission wavelengths were 480 and 520 nm, respectively. Concentrations used: TMR-5′-cTAR-3′-Fl, 0.1 μM; Ac-HKWPWW-NH_2, 7 μM; NC(12−55), 1.1 μM. The fluorescence lifetimes, τ_1 to τ_3, the relative amplitudes, α_1 to α_3, and the mean lifetime, $\langle\tau\rangle$, are expressed as means for three experiments. The relative amplitude, α_0, of the dark species and the remaining amplitudes, α_{ic}, were recalculated as in Table 1.

the modest shift observed with Trp5 suggests that this residue is only moderately involved in the complexes formed with this peptide conformation. A more symmetric situation was observed with the *trans*-Pro conformation, since the three Trp residues displayed comparable chemical shifts during their interaction with (−)PBS. Nevertheless, since at all peptide:oligonucleotide ratios, the changes in the chemical shifts of Trp5 were systematically higher than those of Trp3 and Trp6, this suggests that Trp5 may contribute slightly more than the two other Trp residues in the complexes of the *trans*-Pro conformation with (−)PBS. Moreover, since time-resolved fluorescence data show that only a fraction of the Trp residues is involved in stacking interactions, the binding of both peptide conformations is probably heterogeneous with the number and nature of stacked Trp residues differing from one bound peptide to another.

Ac-HKWPWW-NH_2 Stabilizes the Secondary Structure of PBS and cTAR. Since Ac-HKWPWW-NH_2 binds to TAR and PBS with affinities similar to that of NC, this prompted us to determine if, by analogy to NC, the peptide exhibits nucleic acid chaperone activities. To this end, we analyzed the interaction of Ac-HKWPWW-NH_2 with cTAR doubly labeled at its 5′ and 3′ ends by TMR and Fl, respectively. As previously shown, the TMR and Fl dyes form a nonfluorescent heterodimer when the stem of cTAR is closed (*10*, *38*). However, due to fraying of the terminal bases of cTAR stem, the nonfluorescent closed species was shown to be in equilibrium with partly melted fluorescent species (where Fl was removed away from TMR) (*10*, *38*, *39*). Since, in melted species, Fl and TMR undergo FRET, the time-resolved fluorescence technique has been shown to accurately identify the melting degree of the various species in solution, as well as their population (*10*). In this respect, the three lifetime components, τ_1 to τ_3, of TMR-5′-cTAR-3′-Fl (Table 4) have been associated with the melting of the terminal 3 bp segment, the lower half of cTAR, and the whole cTAR molecule, respectively (*10*, *38*). These partly melted species are in equilibrium with a population, α_0, of closed dark species (associated with a null lifetime) representing 73% in the present batch of cTAR molecules. NC shifted the equilibrium toward the partly melted species (as could be seen from the increase in α_1 to α_3 values), increasing the fluorescence intensity of TMR-5′-cTAR-3′-Fl by a factor of about 3 (Table 4). In sharp contrast, addition of increasing concentrations of Ac-HKWPWW-NH_2 induced a fluorescence decrease (amounting to about 20% in the presence of an excess of peptide) with no significant change in the ratio of the Fl to TMR peaks (Figure 7a). This fluorescence decrease is due to a significant increase of the α_0 value at the expense of all other species, suggesting that Ac-HKWPWW-NH_2 decreases the population of melted species to the benefit of the dark species and thus that the peptide stabilizes the cTAR secondary structure. Interestingly, Ac-HKWPWW-NH_2 induced also a decrease of the fluorescence intensity (by about 8%) at 37 °C, although to a lesser extent than at 20 °C.

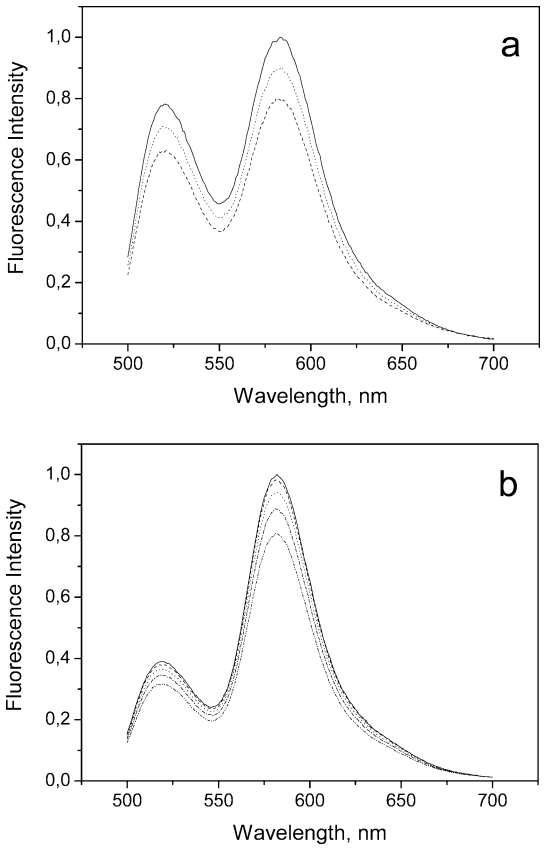

FIGURE 7: Stabilization by Ac-HKWPWW-NH_2 of the secondary structures of cTAR and (−)PBS. (a) The fluorescence spectrum of TMR-5′-cTAR-3′-Fl (100 nM) was recorded in the absence (solid line) or in the presence of Ac-HKWPWW-NH_2 at a concentration of 5 μM (dotted line) or 10 μM (dashed line), respectively. (b) Fluorescence spectra of 100 nM TMR-5′-(−)PBS-3′-Fl in the absence (solid line) and in the presence (dotted lines) of 1, 2, 5, and 10 μM Ac-HKWPWW-NH_2.

In a next step, we analyzed the interaction of Ac-HKWPWW-NH_2 with TMR-5′-(−)PBS-3′-Fl. This oligonucleotide was also shown to be in equilibrium between closed and open species (*9*, *60*). In contrast to cTAR, NC has been shown to induce only a limited 1.4-fold increase in TMR-5′-(−)PBS-3′-Fl fluorescence, due to a limited redistribution between the already partly opened species. As for cTAR, addition of an excess of Ac-HKWPWW-NH_2 decreases the fluorescence of TMR-5′-(−)PBS-3′-Fl by about 20% (Figure 7b), suggesting that Ac-HKWPWW-NH_2 also stabilizes the secondary structure of the PBS. The absence

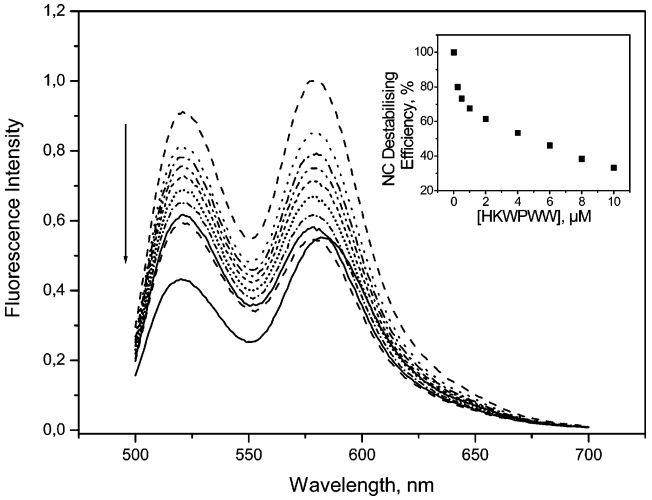

FIGURE 8: Inhibition by Ac-HKWPWW-NH_2 of NC(12−55) destabilizing activity. The bottom spectrum (solid line) and top spectrum (dashed line) correspond to 100 nM TMR-5′-cTAR-3′-Fl in the absence and the presence of 1.1 μM NC(12−55), respectively. The dotted lines describe the spectra of the TMR-5′-cTAR-3′-Fl/NC(12−55) complexes in the presence of increasing concentrations (as indicated by the arrow) of Ac-HKWPWW-NH_2. Inset: Inhibition by Ac-HKWPWW-NH_2 of the NC(12−55)-directed destabilization of cTAR. The inhibition was calculated on basis of the Fl peak intensity of TMR-5′-cTAR-3′-Fl.

of Ac-HKWPWW-NH_2-promoted destabilization of (−)PBS stem is further supported by the absence of changes in the chemical shift, line width, and relative intensity of the imino proton signals of the four (−)PBS base pairs in the NMR titration.

Ac-HKWPWW-NH_2 Inhibits NC-Directed Destabilization of cTAR. Since Ac-HKWPWW-NH_2 and NC(12−55) show similar binding affinities but opposite effects on cTAR stability, we examined the competing effect of Ac-HKWPWW-NH_2 on NC-directed destabilization of cTAR secondary structure. For these experiments, 100 nM TMR-5′-cTAR-3′-Fl was first incubated with NC(12−55) at a nucleotide to protein molar ratio of 5. As shown in Figure 8, this results in a sharp fluorescence intensity increase due to the partial melting of cTAR secondary structure. Addition of increasing concentrations of Ac-HKWPWW-NH_2 gradually reduces the fluorescence intensity of both Fl and TMR peaks, suggesting that Ac-HKWPWW-NH_2 competitively inhibits NC destabilizing activity. At the highest concentration (10 μM) of Ac-HKWPWW-NH_2, the intensity of the Fl peak was still 40% higher than the Fl intensity in the free oligonucleotide, while the intensity of the TMR peak was reduced to the level of the TMR peak in the free oligonucleotide. This indicates that the FRET between Fl and TMR was reduced with respect to that in the free oligonucleotide and, thus, that cTAR equilibrium is still partly shifted toward the melted forms. In line with this partial inhibition of NC destabilizing activity, the time-resolved measurements showed that in the presence of both peptides the amplitude of the closed species (α_0) and the amplitudes of the partly melted species (α_1 to α_3) were intermediate to those of the free cTAR and the cTAR/NC complexes (Table 4). Taken together, our data indicate that Ac-HKWPWW-NH_2 inhibits NC destabilizing activity, probably by competing with NC for binding cTAR. This competition between NC and Ac-HKWPWW-NH_2 for binding cTAR was further confirmed by adding increasing NC concentrations to a cTAR−Ac-HKWPWW-NH_2 complex. We observed a clear fluorescence increase of TMR-5′-cTAR-3′-Fl fluorescence, indicating that NC(12−55) displaces Ac-HKWPWW-NH_2 and exerts its destabilizing activity (data not shown). On the basis of these conclusions, the EC_{50} concentration of Ac-HKWPWW-NH_2 that inhibits 50% of the NC destabilizing activity (under the conditions described in the legend of Figure 8) was found to be about 4 μM as determined from the Fl intensity peak (Figure 8, inset). Interestingly, the effect of Ac-HKWPWW-NH_2 on NC destabilizing activity at 37 °C was similar to that described at 20 °C, with an EC_{50} of 3.5 μM, indicating that the competing effect of the peptide is preserved at physiological temperature.

DISCUSSION

In the present work, we characterized the structure and the fluorescence properties of Ac-HKWPWW-NH_2 and its potency to inhibit NC destabilizing activity. After structural calculations and free energy minimization, a well-defined structure was found around the central Pro residue. Moreover, the peptide was found to exhibit two slowly interconverting conformations that were attributed to *cis*- and *trans*-Pro conformations. In contrast to His1, Lys2, and Trp6 residues which showed no preferred orientation, Trp3 and Trp5 adopted defined orientations in both conformations. In the *trans*-Pro conformation, the proximity of Trp3 and Trp5 indole rings as well as their planar orientation suggests a stacking interaction between the two indole rings. Such an interaction may also exist between Trp3 and Trp6 side chains in the *trans* conformation as well as between Trp5 and Trp6 in the *cis* conformation. Since fluorescence quenching due to ground state stacking interactions has been reported for various fluorescence pairs (*61*−*63*), stacking interactions between Trp side chains may explain the low quantum yield of the peptide as well as the static fluorescence quenching (Table 1). As described by the exciton theory, these ground state interactions between parallel Trp side chains in an H-type geometry [in which the transition dipoles of the individual chromophores are parallel to each other and normal to the radius vector connecting them (*64*)] probably allow strong coupling between the transition dipoles of the Trp side chains and delocalization of excitation over them, preventing fluorescence emission (*64*−*66*). In contrast, since Lys, Pro, and deprotonated His residues are poor quenchers of Trp fluorescence (ref *55* and references cited therein), these residues probably do not significantly contribute to the low quantum yield of Ac-HKWPWW-NH_2.

Ac-HKWPWW-NH_2 was found to bind with good affinity to both the PBS and TAR viral sequences, confirming the potency of this type of peptide to compete with NC for its target nucleic acid elements (*36*). Since the binding appears to be mainly nonelectrostatic, it is likely that the stacking of the Trp residues with the bases of PBS and TAR derivatives (Tables 2 and 3) governs the binding of Ac-HKWPWW-NH_2 to both PBS and TAR target sequences. In the case of (−)PBS, the two peptide conformations were found to bind with comparable affinities. Though all three Trp residues of Ac-HKWPWW-NH_2 contribute (but not necessarily simultaneously) to the binding of both peptide conformations to (−)PBS, the key residues in the complexes with *cis*-Pro and *trans*-Pro conformations are Trp3 and Trp5, respectively.

This conclusion is in line with the critical role of Trp3 and Trp5 evidenced for the binding to SL3 (*36*). The central contribution of the Trp residues of Ac-HKWPWW-NH_2 in the binding to oligonucleotides is also fully consistent with the critical role of the Trp37 residue of NC, which strongly contributes through its stacking (mainly with guanine residues) (*67*, *68*) to the overall stability of the NC−oligonucleotide complexes (*23*, *58*, *69*). In addition to Trp residues, His1 has also been reported to play an important role in the binding process (*36*). Since His is largely unprotonated at pH 7.5 (Figure 5b), it should thus mainly interact with oligonucleotides through nonelectrostatic interactions.

The good affinity of Ac-HKWPWW-NH_2 for NC nucleic acid targets suggests that it partly mimics the hydrophobic platform formed by the Val13, Phe16, Thr 24, Ala25, Trp37, and Met46 residues in the two folded zinc finger motifs (*11*, *16*). This platform has been shown to be critical for strong binding (*16*, *67*, *68*, *70*, *71*) as well as for nucleic acid destabilization (*23*). This latter property is clearly not realized with Ac-HKWPWW-NH_2 which is unable to destabilize both PBS ad TAR derivatives. This may be attributed to the fact that the proper orientation of the residues in the NC hydrophobic platform is much more critical for destabilization than for binding (*23*). Moreover, the lack of ionic interactions involved in the destabilization properties of NC may also contribute to the inability of the hexapeptide to destabilize the nucleic acids. Due to its flexible structure, Ac-HKWPWW-NH_2 can probably adopt appropriate conformations for binding; however, the subsequent molecular steps related to NC unwinding activity which rely on the constrained structure of the two finger motifs cannot be mimicked by Ac-HKWPWW-NH_2.

In fact, Ac-HKWPWW-NH_2 rather stabilizes both cTAR and PBS secondary structures. Since the stacking of the Trp residues of Ac-HKWPWW-NH_2 with the oligonucleotide bases strongly contributes to the binding affinity, this stacking may also be involved in the stabilization of the oligonucleotides. An exactly opposite conclusion was drawn for NC where the stacking of Trp37 is required to unwind cTAR secondary structure (*23*). This indicates that the destabilization of cTAR by NC probably results from a concerted activity of Trp37 with the other residues of the NC hydrophobic platform that cannot be mimicked by only the Trp residues of the hexapeptide.

Thus, in full line with its good affinity for cTAR, Ac-HKWPWW-NH_2 efficiently inhibits NC destabilizing activity on the cTAR secondary structure (at both 20 and 37 °C) through competition for the same binding sites on cTAR. This suggests that, in addition to its potential interference with the packaging process of HIV-1 RNA genome (*36*), Ac-HKWPWW-NH_2 may potentially interfere with NC during the two-strand transfer reactions in reverse transcription in vivo. This peptide can now serve to derive modified peptides or small molecules with improved binding properties in order to inhibit NC functions during HIV-1 replication.

SUPPORTING INFORMATION AVAILABLE

Expanded Materials and Methods section. This material is available free of charge via the Internet at http://pubs.acs.org.

REFERENCES

1. Clever, J., Sassetti, C., and Parslow, T. G. (1995) RNA secondary structure and binding sites for gag gene products in the 5′ packaging signal of human immunodeficiency virus type 1, *J. Virol. 69*, 2101−2109.
2. Mihailescu, M. R., and Marino, J. P. (2004) A proton-coupled dynamic conformational switch in the HIV-1 dimerization initiation site kissing complex, *Proc. Natl. Acad. Sci. U.S.A. 101*, 1189−1194.
3. Tisne, C., Roques, B. P., and Dardel, F. (2004) The annealing mechanism of HIV-1 reverse transcription primer onto the viral genome, *J. Biol. Chem. 279*, 3588−3595.
4. Lapadat-Tapolsky, M., Gabus, C., Rau, M., and Darlix, J. L. (1997) Possible roles of HIV-1 nucleocapsid protein in the specificity of proviral DNA synthesis and in its variability, *J. Mol. Biol. 268*, 250−260.
5. Levin, J. G., Guo, J., Rouzina, I., and Musier-Forsyth, K. (2005) Nucleic acid chaperone activity of HIV-1 nucleocapsid protein: critical role in reverse transcription and molecular mechanism, *Prog. Nucleic Acid Res. Mol. Biol. 80*, 217−286.
6. Bampi, C., Jacquenet, S., Lener, D., Decimo, D., and Darlix, J. L. (2004) The chaperoning and assistance roles of the HIV-1 nucleocapsid protein in proviral DNA synthesis and maintenance, *Int. J. Biochem. Cell Biol. 36*, 1668−1686.
7. Rein, A., Henderson, L. E., and Levin, J. G. (1998) Nucleic-acid-chaperone activity of retroviral nucleocapsid proteins: significance for viral replication, *Trends Biochem. Sci. 23*, 297−301.
8. Hargittai, M. R., Gorelick, R. J., Rouzina, I., and Musier-Forsyth, K. (2004) Mechanistic insights into the kinetics of HIV-1 nucleocapsid protein-facilitated tRNA annealing to the primer binding site, *J. Mol. Biol. 337*, 951−968.
9. Egele, C., Schaub, E., Ramalanjaona, N., Piemont, E., Ficheux, D., Roques, B., Darlix, J. L., and Mely, Y. (2004) HIV-1 nucleocapsid protein binds to the viral DNA initiation sequences and chaperones their kissing interactions, *J. Mol. Biol. 342*, 453−466.
10. Bernacchi, S., Stoylov, S., Piemont, E., Ficheux, D., Roques, B. P., Darlix, J. L., and Mely, Y. (2002) HIV-1 nucleocapsid protein activates transient melting of least stable parts of the secondary structure of TAR and its complementary sequence, *J. Mol. Biol. 317*, 385−399.
11. Summers, M. F., Henderson, L. E., Chance, M. R., Bess, J. W., Jr., South, T. L., Blake, P. R., Sagi, I., Perez-Alvarado, G., Sowder, R. C., III, Hare, D. R., et al. (1992) Nucleocapsid zinc fingers detected in retroviruses: EXAFS studies of intact viruses and the solution-state structure of the nucleocapsid protein from HIV-1, *Protein Sci. 1*, 563−574.
12. Gorelick, R. J., Gagliardi, T. D., Bosche, W. J., Wiltrout, T. A., Coren, L. V., Chabot, D. J., Lifson, J. D., Henderson, L. E., and Arthur, L. O. (1999) Strict conservation of the retroviral nucleocapsid protein zinc finger is strongly influenced by its role in viral infection processes: characterization of HIV-1 particles containing mutant nucleocapsid zinc-coordinating sequences, *Virology 256*, 92−104.
13. Guo, J., Wu, T., Anderson, J., Kane, B. F., Johnson, D. G., Gorelick, R. J., Henderson, L. E., and Levin, J. G. (2000) Zinc finger structures in the human immunodeficiency virus type 1 nucleocapsid protein facilitate efficient minus- and plus-strand transfer, *J. Virol. 74*, 8980−8988.
14. Berthoux, L., Pechoux, C., and Darlix, J. L. (1999) Multiple effects of an anti-human immunodeficiency virus nucleocapsid inhibitor on virus morphology and replication, *J. Virol. 73*, 10000−10009.
15. Ottmann, M., Gabus, C., and Darlix, J. L. (1995) The central globular domain of the nucleocapsid protein of human immunodeficiency virus type 1 is critical for virion structure and infectivity, *J. Virol. 69*, 1778−1784.
16. Morellet, N., de Rocquigny, H., Mely, Y., Jullian, N., Demene, H., Ottmann, M., Gerard, D., Darlix, J. L., Fournie-Zaluski, M. C., and Roques, B. P. (1994) Conformational behaviour of the active and inactive forms of the nucleocapsid NCp7 of HIV-1 studied by ^{1}H NMR, *J. Mol. Biol. 235*, 287−301.
17. Remy, E., de Rocquigny, H., Petitjean, P., Muriaux, D., Theilleux, V., Paoletti, J., and Roques, B. P. (1998) The annealing of tRNA3Lys to human immunodeficiency virus type 1 primer binding site is critically dependent on the NCp7 zinc fingers structure, *J. Biol. Chem. 273*, 4819−4822.
18. Rong, L., Liang, C., Hsu, M., Kleiman, L., Petitjean, P., de Rocquigny, H., Roques, B. P., and Wainberg, M. A. (1998) Roles

of the human immunodeficiency virus type 1 nucleocapsid protein in annealing and initiation versus elongation in reverse transcription of viral negative-strand strong-stop DNA, *J. Virol. 72*, 9353−9358.
19. Williams, M. C., Rouzina, I., Wenner, J. R., Gorelick, R. J., Musier-Forsyth, K., and Bloomfield, V. A. (2001) Mechanism for nucleic acid chaperone activity of HIV-1 nucleocapsid protein revealed by single molecule stretching, *Proc. Natl. Acad. Sci. U.S.A. 98*, 6121−6126.
20. Guo, J., Wu, T., Kane, B. F., Johnson, D. G., Henderson, L. E., Gorelick, R. J., and Levin, J. G. (2002) Subtle alterations of the native zinc finger structures have dramatic effects on the nucleic acid chaperone activity of human immunodeficiency virus type 1 nucleocapsid protein, *J. Virol. 76*, 4370−4378.
21. Heath, M. J., Derebail, S. S., Gorelick, R. J., and DeStefano, J. J. (2003) Differing roles of the N- and C-terminal zinc fingers in human immunodeficiency virus nucleocapsid protein-enhanced nucleic acid annealing, *J. Biol. Chem. 278*, 30755−30763.
22. Lee, N., Gorelick, R. J., and Musier-Forsyth, K. (2003) Zinc finger-dependent HIV-1 nucleocapsid protein-TAR RNA interactions, *Nucleic Acids Res. 31*, 4847−4855.
23. Beltz, H., Clauss, C., Piemont, E., Ficheux, D., Gorelick, R. J., Roques, B., Gabus, C., Darlix, J. L., de Rocquigny, H., and Mely, Y. (2005) Structural determinants of HIV-1 nucleocapsid protein for cTAR DNA binding and destabilization, and correlation with inhibition of self-primed DNA synthesis, *J. Mol. Biol. 348*, 1113−1126.
24. Williams, M. C., Rouzina, I., and Bloomfield, V. A. (2002) Thermodynamics of DNA interactions from single molecule stretching experiments, *Acc. Chem. Res. 35*, 159−166.
25. De Rocquigny, H., Gabus, C., Vincent, A., Fournie-Zaluski, M. C., Roques, B., and Darlix, J. L. (1992) Viral RNA annealing activities of human immunodeficiency virus type 1 nucleocapsid protein require only peptide domains outside the zinc fingers, *Proc. Natl. Acad. Sci. U.S.A. 89*, 6472−6476.
26. Mayasundari, A., Rice, W. G., Diminnie, J. B., and Baker, D. C. (2003) Synthesis, resolution, and determination of the absolute configuration of the enantiomers of *cis*-4,5-dihydroxy-1,2-dithiane 1,1-dioxide, an HIV-1NCp7 inhibitor, *Bioorg. Med. Chem. 11*, 3215−3219.
27. Basrur, V., Song, Y., Mazur, S. J., Higashimoto, Y., Turpin, J. A., Rice, W. G., Inman, J. K., and Appella, E. (2000) Inactivation of HIV-1 nucleocapsid protein P7 by pyridinioalkanoyl thioesters. Characterization of reaction products and proposed mechanism of action, *J. Biol. Chem. 275*, 14890−14897.
28. Gorelick, R. J., Benveniste, R. E., Lifson, J. D., Yovandich, J. L., Morton, W. R., Kuller, L., Flynn, B. M., Fisher, B. A., Rossio, J. L., Piatak, M., Jr., Bess, J. W., Jr., Henderson, L. E., and Arthur, L. O. (2000) Protection of Macaca nemestrina from disease following pathogenic simian immunodeficiency virus (SIV) challenge: utilization of SIV nucleocapsid mutant DNA vaccines with and without an SIV protein boost, *J. Virol. 74*, 11935−11949.
29. Druillennec, S., Meudal, H., Roques, B. P., and Fournie-Zaluski, M. C. (1999) Nucleomimetic strategy for the inhibition of HIV-1 nucleocapsid protein NCp7 activities, *Bioorg. Med. Chem. Lett. 9*, 627−632.
30. Darlix, J. L., Cristofari, G., Rau, M., Pechoux, C., Berthoux, L., and Roques, B. (2000) Nucleocapsid protein of human immunodeficiency virus as a model protein with chaperoning functions and as a target for antiviral drugs, *Adv. Pharmacol. 48*, 345−372.
31. Rice, W. G., Supko, J. G., Malspeis, L., Buckheit, R. W., Jr., Clanton, D., Bu, M., Graham, L., Schaeffer, C. A., Turpin, J. A., Domagala, J., Gogliotti, R., Bader, J. P., Halliday, S. M., Coren, L., Sowder, R. C., II, Arthur, L. O., and Henderson, L. E. (1995) Inhibitors of HIV nucleocapsid protein zinc fingers as candidates for the treatment of AIDS, *Science 270*, 1194−1197.
32. Allen, P., Collins, B., Brown, D., Hostomsky, Z., and Gold, L. (1996) A specific RNA structural motif mediates high affinity binding by the HIV-1 nucleocapsid protein (NCp7), *Virology 225*, 306−315.
33. Stephen, A. G., Worthy, K. M., Towler, E., Mikovits, J. A., Sei, S., Roberts, P., Yang, Q. E., Akee, R. K., Klausmeyer, P., McCloud, T. G., Henderson, L., Rein, A., Covell, D. G., Currens, M., Shoemaker, R. H., and Fisher, R. J. (2002) Identification of HIV-1 nucleocapsid protein: nucleic acid antagonists with cellular anti-HIV activity, *Biochem. Biophys. Res. Commun. 296*, 1228−1237.
34. Berglund, J. A., Charpentier, B., and Rosbash, M. (1997) A high affinity binding site for the HIV-1 nucleocapsid protein, *Nucleic Acids Res. 25*, 1042−1049.
35. Kim, M. Y., and Jeong, S. (2003) RNA aptamers that bind the nucleocapsid protein contain pseudoknots, *Mol. Cells 16*, 413−417.
36. Pustowka, A., Dietz, J., Ferner, J., Baumann, M., Landersz, M., Konigs, C., Schwalbe, H., and Dietrich, U. (2003) Identification of peptide ligands for target RNA structures derived from the HIV-1 packaging signal psi by screening phage-displayed peptide libraries, *ChemBioChem 4*, 1093−1097.
37. de Rocquigny, H., Ficheux, D., Gabus, C., Fournie-Zaluski, M. C., Darlix, J. L., and Roques, B. P. (1991) First large scale chemical synthesis of the 72 amino acid HIV-1 nucleocapsid protein NCp7 in an active form, *Biochem. Biophys. Res. Commun. 180*, 1010−1018.
38. Beltz, H., Azoulay, J., Bernacchi, S., Clamme, J. P., Ficheux, D., Roques, B., Darlix, J. L., and Mely, Y. (2003) Impact of the terminal bulges of HIV-1 cTAR DNA on its stability and the destabilizing activity of the nucleocapsid protein NCp7, *J. Mol. Biol. 328*, 95−108.
39. Azoulay, J., Clamme, J. P., Darlix, J. L., Roques, B. P., and Mely, Y. (2003) Destabilization of the HIV-1 complementary sequence of TAR by the nucleocapsid protein through activation of conformational fluctuations, *J. Mol. Biol. 326*, 691−700.
40. Bodenhausen, G., and Ruben, D. J. (1980) Natural abundance nitrogen-15 NMR by enhanced heteronuclear spectroscopy, *Chem. Phys. Lett. 69*, 185−189.
41. Cavanagh, J., Palmer, A. G., III, Wright, P. E., and Rance, M. (1991) Sensitivity improvement in proton-detected 2-dimensional heteronuclear relay spectroscopy, *J. Magn. Reson. 91*, 429−436.
42. Kay, L. E., Keifer, P., and Saarinen, T. (1992) Pure absorption gradient enhanced heteronuclear single quantum correlation spectroscopy with improved sensitivity, *J. Am. Chem. Soc. 114*, 10663−10665.
43. Braunschweiler, L., and Ernst, R. R. (1983) Coherence transfer by isotropic mixing: application to proton correlation spectroscopy, *J. Magn. Reson. 53*, 521−528.
44. Bothner-By, A. A., and Noggle, J. H. (1979) Time development of nuclear Overhauser effects in multispin systems, *J. Am. Chem. Soc. 101*, 5152−5155.
45. Brunger, A. T., Adams, P. D., Clore, G. M., DeLano, W. L., Gros, P., Grosse-Kunstleve, R. W., Jiang, J. S., Kuszewski, J., Nilges, M., Pannu, N. S., Read, R. J., Rice, L. M., Simonson, T., and Warren, G. L. (1998) Crystallography & NMR system: A new software suite for macromolecular structure determination, *Acta Crystallogr., Sect. D: Biol. Crystallogr. 54* (*Part 5*), 905−921.
46. Linge, J. P., O'Donoghue, S. I., and Nilges, M. (2001) Automated assignment of ambiguous nuclear overhauser effects with ARIA, *Methods Enzymol. 339*, 71−90.
47. Linge, J. P., O'Donoghue, S. I., and Nilges, M. (1999) Influence of non-bonded parameters on the quality of NMR structures: a new force field for NMR structure calculation, *J. Biomol. NMR 13*, 51−59.
48. Eisinger, J., and Navon, G. (1969) Fluorescence quenching and isotope effect of tryptophan, *J. Chem. Phys. 50*, 2069−2077.
49. Livesey, A. K., and Brochon, J. C. (1987) Analyzing the distribution of decay constants in pulse-fluorimetry using the maximum entropy method, *Biophys. J. 67*, 2013−2023.
50. Lee, Y. C., Jackson, P. L., Jablonsky, M. J., Muccio, D. D., Pfister, R. R., Haddox, J. L., Sommers, C. I., Anantharamaiah, G. M., and Chaddha, M. (2001) NMR conformational analysis of cis and trans proline isomers in the neutrophil chemoattractant, *N*-acetyl-proline-glycine-proline, *Biopolymers 58*, 548−561.
51. Schubert, M., Labudde, D., Oschkinat, H., and Schmieder, P. (2002) A software tool for the prediction of Xaa-Pro peptide bond conformations in proteins based on ^{13}C chemical shift statistics, *J. Biomol. NMR 24*, 149−154.
52. Lakowicz, J. R. (1999) *Principles of Fluorescence Spectroscopy*, 2nd ed., Plenum Publishing, New York.
53. Werner, T. C., and Forster, L. S. (1979) The fluorescence of tryptophanyl peptides, *Photochem. Photobiol. 29*, 905−914.
54. Shinitzky, M., and Goldman, R. (1967) Fluorometric detection of histiine-tryptophan complexes in peptides and proteins, *Eur. J. Biochem. 3*, 139−144.
55. Chen, Y., and Barkley, M. D. (1998) Toward understanding tryptophan fluorescence in proteins, *Biochemistry 37*, 9976−9982.
56. Mely, Y., Cornille, F., Fournie-Zaluski, M. C., Darlix, J. L., Roques, B. P., and Gerard, D. (1991) Investigation of zinc-binding

affinities of Moloney murine leukemia virus nucleocapsid protein and its related zinc finger and modified peptides, *Biopolymers 31*, 899−906.

57. Montenay-Garestier, T., Toulme, F., Fidy, J., Toulme, J.-J., and Le Doan, T. (1983) in *Structure, Dynamics and Interactions and Evolution of Biological Macromolecules* (Helene, C., Ed.) pp 113−128, D. Reidel Publishing Co., Dordrecht, The Netherlands.
58. Bombarda, E., Ababou, A., Vuilleumier, C., Gerard, D., Roques, B. P., Piemont, E., and Mely, Y. (1999) Time-resolved fluorescence investigation of the human immunodeficiency virus type 1 nucleocapsid protein: influence of the binding of nucleic acids, *Biophys. J. 76*, 1561−1570.
59. Record, M. T., Lohman, M. L., and De Haseth, P. (1976) Ion effects on ligand-nucleic acid interactions, *J. Mol. Biol. 107*, 145−158.
60. Egele, C., Schaub, E., Piemont, E., de Rocquigny, H., and Mely, Y. (2005) Investigation by fluorescence correlation spectroscopy of the chaperoning interactions of HIV-1 nucleocapsid protein with the viral DNA initiation sequences, *C. R. Biol. 328*, 1041−1051.
61. Geoghegan, K. F., Rosner, P. J., and Hoth, L. R. (2000) Dye-pair reporter systems for protein-peptide molecular interactions, *Bioconjugate Chem. 11*, 71−77.
62. Krishnamoorthy, G., Roques, B., Darlix, J. L., and Mely, Y. (2003) DNA condensation by the nucleocapsid protein of HIV-1: a mechanism ensuring DNA protection, *Nucleic Acids Res. 31*, 5425−5432.
63. Packard, B. Z., Toptygin, D. D., Komoriya, A., and Brand, L. (1997) Design of profluorescent protease substrates guided by exciton theory, *Methods Enzymol. 278*, 15−23.
64. Kasha, M. (1963) Energy transfer mechanisms and the molecular exciton model for molecular composite systems, *Radiat. Res. 20*, 55−71.
65. Kasha, M. (1991) Energy transfer, charge transfer, and proton transfer in molecular composite systems, *Basic Life Sci. 58*, 231−251.
66. Scholes, D. S., and Ghiggino, K. P. (1994) Electronic interactions and interchromophore excitation transfer, *J. Phys. Chem. 98*, 4580−4590.
67. De Guzman, R. N., Wu, Z. R., Stalling, C. C., Pappalardo, L., Borer, P. N., and Summers, M. F. (1998) Structure of the HIV-1 nucleocapsid protein bound to the SL3 psi-RNA recognition element, *Science 279*, 384−388.
68. Morellet, N., Demene, H., Teilleux, V., Huynh-Dinh, T., de Rocquigny, H., Fournie-Zaluski, M. C., and Roques, B. P. (1998) Structure of the complex between the HIV-1 nucleocapsid protein NCp7 and the single-stranded pentanucleotide d(ACGCC), *J. Mol. Biol. 283*, 419−434.
69. Vuilleumier, C., Bombarda, E., Morellet, N., Gerard, D., Roques, B. P., and Mely, Y. (1999) Nucleic acid sequence discrimination by the HIV-1 nucleocapsid protein NCp7: a fluorescence study, *Biochemistry 38*, 16816−16825.
70. Amarasinghe, G. K., De Guzman, R. N., Turner, R. B., and Summers, M. F. (2000) NMR structure of stem-loop SL2 of the HIV-1 psi RNA packaging signal reveals a novel A-U-A base-triple platform, *J. Mol. Biol. 299*, 145−156.
71. Stote, R. H., Kellenberger, E., Muller, H., Bombarda, E., Roques, B. P., Kieffer, B., and Mely, Y. (2004) Structure of the His44 → Ala single point mutant of the distal finger motif of HIV-1 nucleocapsid protein: a combined NMR, molecular dynamics simulation, and fluorescence study, *Biochemistry 43*, 7687−7697.
72. Baudin, F., Marquet, R., Isel, C., Darlix, J. L., Ehresmann, B., and Ehresmann, C. (1993) Functional sites in the 5′ region of human immunodeficiency virus type 1 RNA form defined structural domains, *J. Mol. Biol. 229*, 382−397.
73. Johnson, P. E., Turner, R. B., Wu, Z. R., Hairston, L., Guo, J., Levin, J. G., and Summers, M. F. (2000) A mechanism for plus-strand transfer enhancement by the HIV-1 nucleocapsid protein during reverse transcription, *Biochemistry 39*, 9084−9091.
74. SantaLucia, J., Jr. (1998) A unified view of polymer, dumbbell, and oligonucleotide DNA nearest-neighbor thermodynamics, *Proc. Natl. Acad. Sci. U.S.A. 95*, 1460−1465.

BI052560M